Rare Met. (2022) 41(6):2108–2117
https://doi.org/10.1007/s12598-021-01882-2

RARE METALS

ORIGINAL ARTICLE

Nanosized Rh grown on single-walled carbon nanohorns for efficient methanol oxidation reaction

Xiang-Jie Guo, Qi Zhang, Ya-Nan Li, Yang Chen, Lu Yang, Hai-Yan He, Xing-Tao Xu, Hua-Jie Huang*

Received: 2 August 2021 / Revised: 1 September 2021 / Accepted: 6 September 2021 / Published online: 15 January 2022

Abstract Reasonable design and controllable synthesis of non-Pt catalysts with high methanol oxidation activity are regarded as a valid way to promote the large-scale commercial applications of direct methanol fuel cells (DMFCs). Herein, we develop a convenient and cost-effective approach to the successful fabrication of nanosized Rh grown on single-walled carbon nanohorns (Rh/SWCNH) as anode catalysts for DMFCs. The unique architectural configuration endows the as-obtained hybrids with a series of intriguing structural merits, including large specific surface areas, abundant opened holes, optimized electronic structures, homogeneous Rh dispersion, and good electrical conductivity. As a consequence, the resulting Rh/SWCNH catalysts exhibit exceptional electrocatalytic properties in terms of a large electrochemically active surface area of 102.5 $m^2 \cdot g^{-1}$, a high mass activity of 784.0 $mA \cdot mg^{-1}$, as well as reliable long-term durability towards the methanol oxidation reaction in alkaline media, thereby holding great potential as alternatives for commercial Pt/carbon black and Pd/carbon black catalysts.

Keywords Rhodium; Carbon nanohorns; Electrocatalysts; Methanol oxidation; Fuel cells

1 Introduction

Along with the growing public awareness of energy conservation and environment protection, the development of high-efficiency and clean energy conversion technologies have attracted widespread attention in the past few years [1–4]. In particular, the fuel cell systems are able to directly convert the chemical energy of fuels into electric energy, which has broad application prospects in aerospace, electric vehicles, and portable electronic equipment [5–7]. Among various kinds of fuel cells, direct methanol fuel cells (DMFCs) have some unique characteristics such as high energy-conversion efficiency, low pollution emissions, concise structural design, and convenient storage and transportation of the liquid methanol [8–10]. However, the inherently sluggish kinetics of methanol oxidation reaction at the anode seriously hampers the overall power density of the DMFCs, which highlights the need for the exploration and utilization of highly active electrode catalysts [11–13].

As is well known, platinum (Pt) and its derivatives possess unique electrocatalytic activity towards the methanol oxidation, while their scarcity and high prices largely increase the overall manufacturing costs of the fuel cells [14–16]. Meanwhile, Pt atoms easily adsorb the intermediate carbonaceous species (mainly CO) arising from the incomplete methanol oxidation process, which would significantly deteriorate the catalytic ability of the Pt-based catalysts [17–19]. In view of these problems, the development of non-Pt catalysts with acceptable cost and strong anti-poisoning capacity has aroused extensive research interests [20–23]. Recently, the use of rhodium

Supplementary Information The online version contains supplementary material available at https://doi.org/10.1007/s12598-021-01882-2.

X.-J. Guo, Q. Zhang, Y.-N. Li, Y. Chen, L. Yang, H.-Y. He, H.-J. Huang*
College of Mechanics and Materials, Hohai University, Nanjing 210098, China
e-mail: huanghuajie@hhu.edu.cn

X.-T. Xu
International Center for Materials Nanoarchitectonics (WPI-MANA), National Institute for Materials Science, Ibaraki 305-0044, Japan

(Rh) nanocrystals as fuel cell catalysts have become a hot topic due to their superior electrocatalytic activity in alkaline mediums as well as greater resistance to CO in comparison with the Pt catalysts [24–26]. Noteworthy, as a noble metal, the amount of metal Rh in the fuel cell systems must be minimized in order to match the requirements of commercial production. Therefore, it is indispensable to prepare small-sized and well-dispersed Rh catalysts with advanced architectural design to achieve a high Rh utilization efficiency.

Combining noble metal nanocrystals with various supporting materials has long been regarded as an efficient strategy to reduce their usage as well as improve the catalytic performance [27–29]. Specially, with continual advances in nanotechnology, carbonaceous nanomaterials with large specific surface areas and high electrical conductivity have been demonstrated as high-quality supports for dispersing noble metal catalysts [30, 31]. Nonetheless, conventional carbon nanomaterials, such as carbon nanofiber, carbon nanotubes, and graphene, commonly lack adequate and rational porous structures, which is unfavorable for the rapid transport of the methanol electrolyte to the internal metal active sites [32, 33]. Moreover, due to their high graphitization degrees, most pristine carbon nanomaterials are electrochemically inert and thereby cannot directly engage in the electrocatalytic processes [34–36].

As a rising star in the low-dimensional carbon family, single-walled carbon nanohorns (SWCNHs) have shown a number of structural advantages in comparison with conventional nanocarbons [37, 38]. Specifically, SWCNHs are horn-shaped single-walled tubules with plenty of open holes, which are able to serve as ideal platforms for the nucleation and growth of noble metal nanoparticles and simultaneously provide numerous channels for the fast diffusion of external electrolytes [39, 40]. In addition, both theoretical and experimental investigations have revealed that the carbon atoms distributed at the conical tip positions of SWCNHs are more reactive than those at the basal plane positions, thereby leading to improved electrocatalytic ability [41, 42]. Therefore, it is of great interest to explore the possibility of Rh nanocrystals/SWCNH hybrid, which is expected to dramatically enhance the methanol oxidation performance as a result of strong concerted effects between the components. To our knowledge, neither fabrication nor electrocatalytic properties of this intriguing nanostructure have been reported so far.

In this study, we report a convenient and cost-effective approach to the synthesis of nanosized Rh grown on SWCNHs (Rh/SWCNH) as anode catalysts towards methanol oxidation reaction. The formation procedures leading to the Rh/SWCNH hybrids are illustrated in Fig. 1.

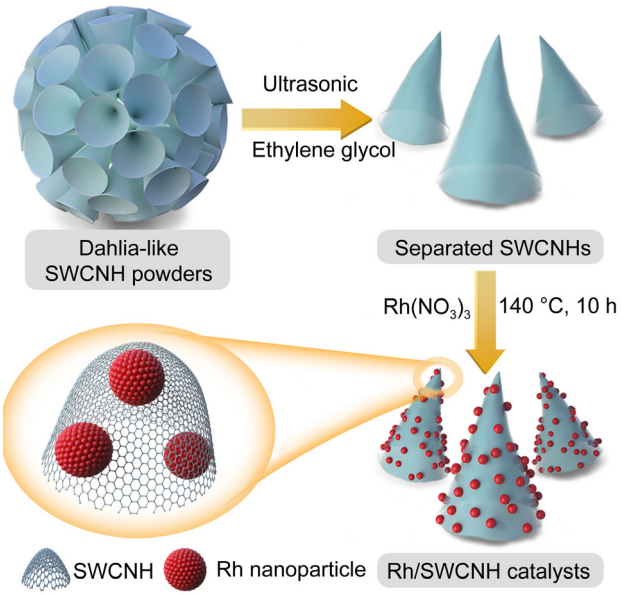

Fig. 1 Schematic illustration of synthetic procedures for Rh/SWCNH architecture

As the starting material, pristine SWCNHs are made up of single-layered graphene with sp^2 carbon atoms, which tend to spontaneously assemble to form a "dahlia-like" spherical architecture with a large number of opened holes. After ultrasonic treatment, the separated SWCNHs can be well dispersed in the ethylene glycol solution to form a uniform black suspension. Subsequently, the introduction of the $Rh(NO_3)_3$ solution enables the growth of Rh nanoparticles on both the internal and external surfaces of SWCNHs under the solvothermal condition, giving birth to the Rh/SWCNH catalysts. Benefiting from the large specific surface area, interconnected open-pore nanostructure, optimized electronic structures, homogeneous Rh dispersion, and high electrical conductivity, the resulting Rh/SWCNH catalysts express unusual electrocatalytic properties towards methanol oxidation reaction, including large electrochemically active surface area, high mass/specific activity, and reliable durability, all of which are significantly superior to those of traditional Rh/carbon black (Rh/C), Rh/carbon nanotube (Rh/CNT), Rh/reduced graphene oxide (Rh/RGO) as well as Pt/C and Pd/C catalysts with the same noble metal loading.

2 Experimental

2.1 Chemicals and materials

Commercial SWCNHs (Nanjing XFNANO Materials Tech Co., Ltd), CNTs (CAS Chengdu Organic Chemistry Co., Ltd), graphene oxide (Nanjing XFNANO Materials

Tech Co., Ltd), carbon black (Vulcan XC-72R, Cabot Corp.), $Rh(NO_3)_3$ (Shanghai Jiuling Chemical Co., Ltd), K_2PtCl_4 (Alfa Aesar), and $Pd(NO_3)_2$ (Alfa Aesar) were directly used as received without further purification.

2.2 Synthesis of Rh/SWCNH catalysts

A facile and cost-effective solvothermal method was developed to prepare the Rh/SWCNH catalysts with various Rh contents (10.0 wt%, 20.0 wt%, 30.0 wt%, and 40.0 wt%). The typical procedures, for instance, when the Rh content is 20.0 wt%, are as follows: 10 mg SWCNH powder was first added into 40 ml ethylene glycol and 40 ml deionized water, and then kept ultrasonic treatment for 45 min to form a homogeneous black dispersion. Subsequently, 19 μl $Rh(NO_3)_3$ solution (1.28 mol·L^{-1}) was introduced into the SWCNH dispersion under magnetic stirring for 15 min. Afterward, the above reaction system was transferred into a 100 ml Teflon-lined stainless steel autoclave and heated at 140 °C for 10 h. The as-generated product, named as 20%-Rh/SWCNH, was washed, filtered, and finally collected with the help of vacuum freeze drying. By adjusting the dosage of $Rh(NO_3)_3$ solution, the controllable fabrication of the 10%-Rh/SWCNH, 30%-Rh/SWCNH, and 40%-Rh/SWCNH catalysts was also achieved. For the purpose of comparison, the same approach was employed to load Rh nanoparticles on the conventional carbon black, CNT, and RGO supports, and the resulting materials were named as 20%-Rh/C, 20%-Rh/CNT, and 20%-Rh/RGO, respectively. Similarly, Pt and Pd nanoparticles were also anchored onto the conventional carbon black support by the use of K_2PtCl_4 and $Pd(NO_3)_2$ as metal precursors through the above approach, and the obtained materials were named as 20%-Pt/C and 20%-Pd/C, respectively.

2.3 Characterization

The microstructure and morphology of the Rh/SWCNH hybrid were investigated by field emission scanning electron microscopy (FESEM, JEOL 6500F) and transmission electron microscopy (TEM, JEOL JEM-2100) equipped with energy dispersive X-ray (EDX) spectroscopy. The crystal textures, composition, and chemical states of the Rh/SWCNH hybrid were studied by X-ray powder diffraction (XRD, Bruker D8 Advance diffractometer with Cu Kα radiation (λ = 0.154 nm)) and X-ray photoelectron spectra (XPS, Perkin Elmer RBD upgraded PHI-5000C ESCA system with Al Kα radiation).

2.4 Electrocatalytic measurements

The electrocatalytic performances of all samples were measured on a CHI 760E electrochemical workstation with a standard three-electrode system at room temperature. In this system, a Pt wire was served as the counter electrode, a saturated calomel electrode (SCE) was used as the reference electrode, and a glassy carbon (GC) disk coated with thin films of catalysts was applied as the working electrode. The GC disk was 3 mm in diameter and 0.07065 cm^2 in geometric area. The preparation procedures of working electrode were as follows: 2 mg catalyst powder was dispersed in a mixed solution containing 475 μl water, 475 μl ethanol, and 50 μl 5% Nafion by sonication for 30 min. Then 5 μl of the above suspension was carefully transferred onto the surface of working electrode and dried naturally before test. The methanol oxidation properties of the Rh/SWCNH as well as reference catalysts were systematically examined by cyclic voltammetry (CV), linear sweep voltammetry (LSV), chronoamperometry and alternating current (AC) impedance techniques in 1 mol·L^{-1} KOH and 1 mol·L^{-1} methanol solution.

3 Results and discussion

The nanostructure and morphology of the as-fabricated Rh/SWCNH hybrid were first observed by means of FESEM and TEM. As shown in Fig. 2a, b, typical FESEM images reveal that the Rh/SWCNH hybrid is composed of numerous horn-shaped tubules with sizes ranging from the nanometer range to several sub-micrometers. Meanwhile, it is found that most nanohorns possess a rough surface, implying the successful deposition of Rh nanoparticles on SWCNHs. Under close inspection by TEM (Fig. 2c–e), the almost transparent SWCNH supports with cone-head structures are decorated uniformly by a large number of Rh nanoparticles with an average diameter of 3.3 nm. Interestingly, with the metal Rh content increasing in the Rh/SWCNH hybrids, more and more nanoparticles with the similar particle sizes (3.2–3.6 nm) are observed to be highly dispersed onto the SWCNH surface (Fig. S1). There is no Rh nanoparticle that is scattered out of the SWCNH supports, suggesting a strong interaction between Rh and support. High-resolution TEM (HRTEM) analysis further discloses that the interplanar spacings of 0.19 and 0.22 nm are assigned to the exposed (200) and (111) planes of cubic Rh nanocrystals, respectively (Fig. 2f, g). Besides, high-angle annular dark-field scanning transmission electron microscopy (HAADF-STEM) image and corresponding elemental mapping images confirm that the Rh/SWCNH

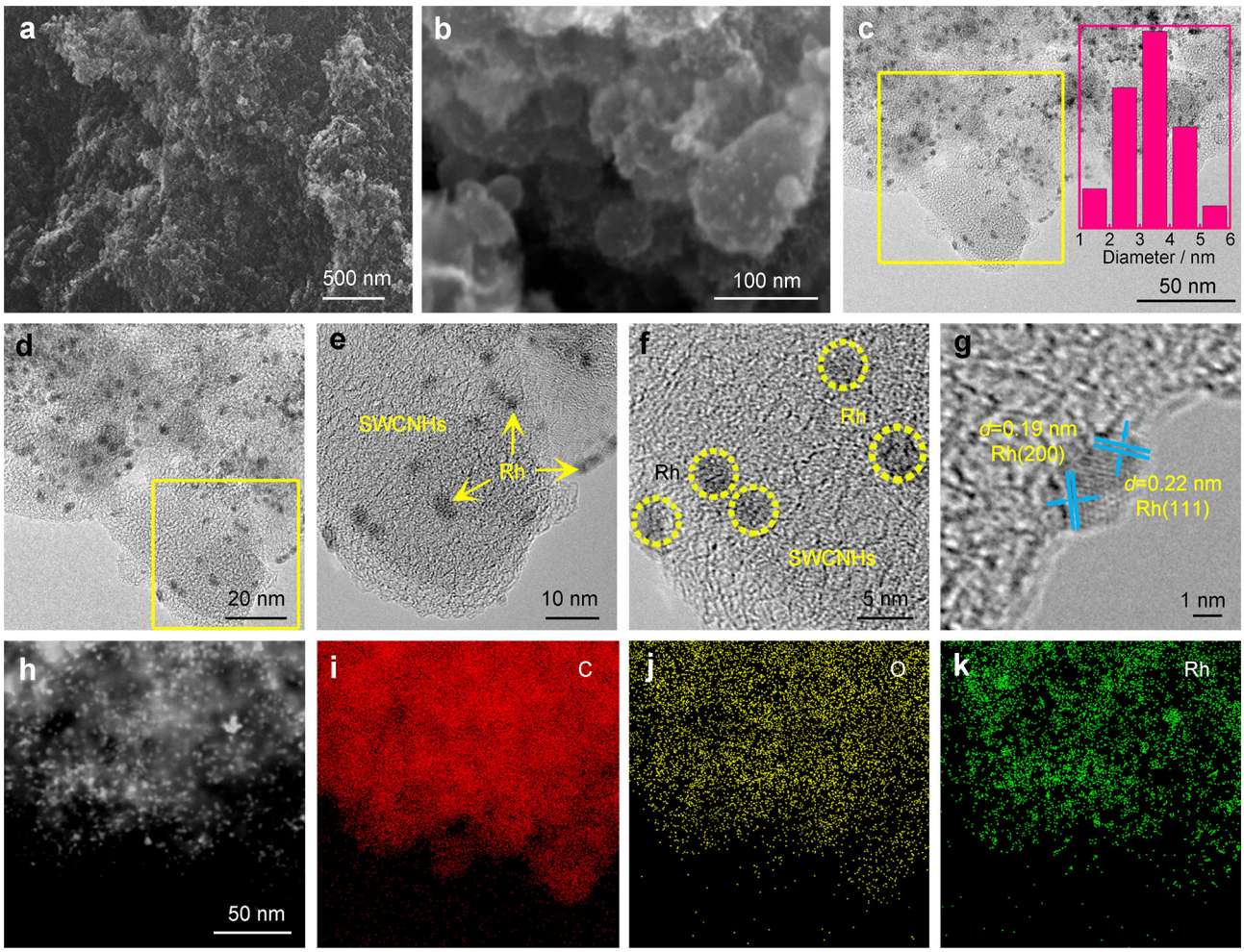

Fig. 2 SEM and TEM analysis of 20%-Rh/SWCNH catalyst: **a**, **b** typical FESEM images, **c**–**e** TEM images (inset in **c** being Rh particle size distribution), and **f**, **g** HRTEM images of Rh/SWCNH catalyst; **h**–**k** HAADF-STEM image and corresponding elemental mapping analysis of C, O, and Rh

hybrid contains C, O, and Rh as the main components (Fig. 2h–k and Fig. S2), which are homogeneously distributed in the architecture.

The crystalline structure and elemental compositions of the Rh/SWCNH hybrid were then investigated by XRD and XPS analysis. Figure 3a depicts typical XRD patterns of Rh/SWCNH, Rh/RGO, Rh/CNT, and Rh/C samples. Clearly, the diffraction peak situated at around $2\theta = 25.0°$ can be detected, which is indexed to the characteristic (002) plane of graphitic SWCNH materials. Meanwhile, other four diffraction peaks centered at $2\theta = 41.1°$, 47.7°, 69.8°, and 84.1° are also visible, corresponding to the (111), (200), (220), and (311) planes of the fcc Rh nanocrystals. In addition, according to the Scherrer equation, the average Rh size of Rh/SWCNH is calculated to be $\sim$ 3.1 nm, which is in good agreement with the above-mentioned TEM result, evidencing that the utilization of SWCNH as support can restrain the overgrowth of Rh nanocrystals. Moreover, XPS elemental analysis verifies that the Rh/SWCNH hybrid is made from C, O, and Rh without any obvious impurities (Fig. S3). The high-resolution C 1s spectrum of Rh/SWCNH shown in Fig. 3b discloses that there are three types of C bonding configurations, consisting of sp^2 C–C, C–OH, and HO-C=O species with binding energies of 284.8, 286.2 and 290.1 eV, respectively. Correspondingly, the complex O 1s spectrum was deconvoluted into three peaks located at 533.5, 532.6, and 531.7 eV (Fig. 3c), which are related to the C–OH, C=O, and HO−C=O groups, respectively [43]. Besides, as displayed in Fig. 3d, the Rh 3d spectrum was resolved into two pairs of energy peaks: the two intensive peaks at 307.7 and 312.5 eV are originated from metallic Rh, while the other two weak peaks at 309.0 and 313.6 eV belong to Rh oxide. Notably, the binding energies for both metallic Rh^0

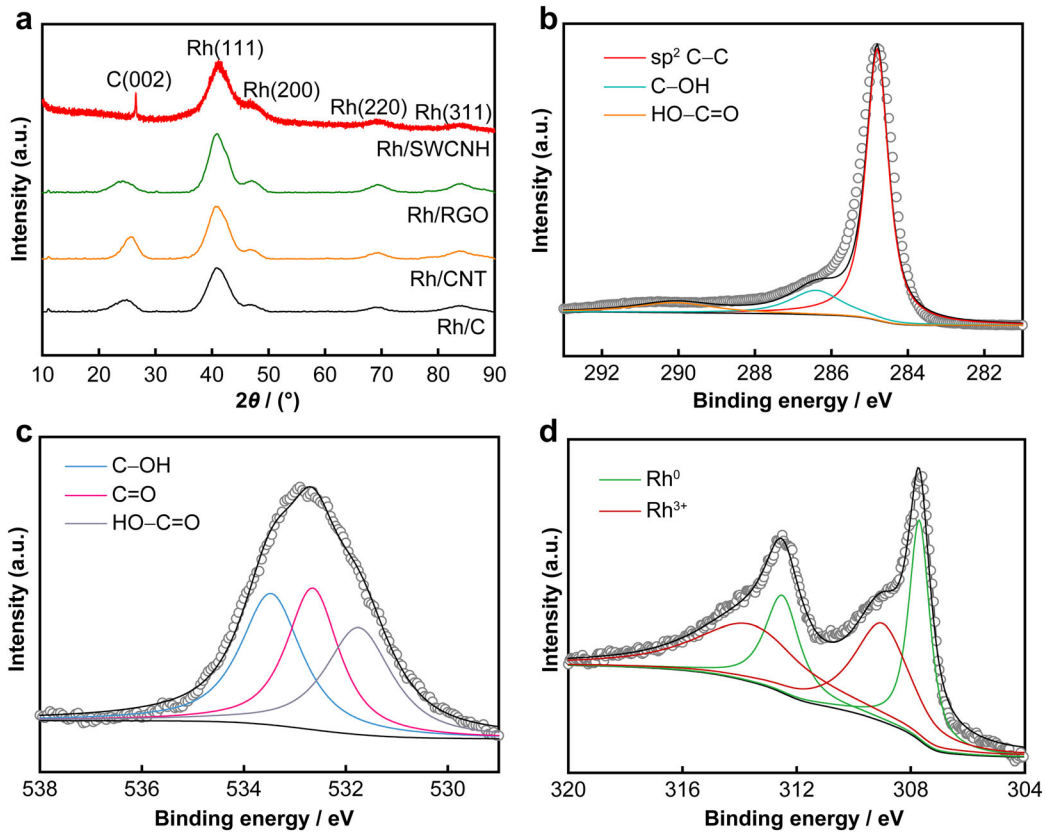

Fig. 3 **a** Representative XRD patterns of Rh/SWCNH, Rh/RGO, Rh/CNT, and Rh/C samples; high-resolution **b** C 1s, **c** O 1s, and **d** Rh 3d XPS spectra of Rh/SWCNH sample

and Rh^{3+} peaks of Rh/SWCNH are shifted negatively with respect to those of Rh/C (Fig. S4), convincingly demonstrating the direct electronic interaction between Rh and SWCNHs, which can lower the mobility of Rh on the SWCNH surface and thereby prevent the agglomeration of Rh nanoparticles.

Inspired by their attractive structural merits, the newly-designed Rh/SWCNH hybrids were coated onto the GC electrodes and measured as anode catalysts towards the methanol oxidation in alkaline medium. CV method was first applied in 1 mol·L^{-1} KOH solution to measure the electrochemically active surface area (ECSA) values of various Rh/SWCNH catalysts with varying Rh loadings. As shown in Fig. 4a, all CV curves exhibit well-defined hydrogen adsorption and desorption peaks in the potential regions from − 0.75 to − 1.05 V. After calculating the hydrogen adsorption peak areas, the 20%-Rh/SWCNH catalyst is found to have the largest ECSA value of up to 102.5 $m^2 \cdot g^{-1}$, followed by 30%-Rh/SWCNH (91.2 $m^2 \cdot g^{-1}$), 40%-Rh/SWCNH (76.4 $m^2 \cdot g^{-1}$), and 10%-Rh/SWCNH (63.2 $m^2 \cdot g^{-1}$). Notably, the ECSA value of 20%-Rh/SWCNH is also remarkably larger than that of 20%-Rh/RGO (52.2 $m^2 \cdot g^{-1}$), 20%-Rh/CNT (44.8 $m^2 \cdot g^{-1}$), and 20%-Rh/C (36.0 $m^2 \cdot g^{-1}$), suggesting that the SWCNH-supported Rh nanocrystals are electrochemically more accessible for catalytic reactions (Fig. 4b, c and Table S1).

The methanol oxidation activities of the different Rh-based catalysts were then evaluated in the presence of 1 mol·L^{-1} KOH and 1 mol·L^{-1} methanol solution. As can be seen from Fig. 4d and Fig. S5, the positive scan of the CV curve is characterized by a prominent methanol oxidation current peak at around − 0.4 V, while the backward current peak at around − 0.7 V is due to the oxidation of the CO byproducts [44]. Remarkably, the methanol oxidation current densities on different Rh/SWCNH electrodes follow the order of 20%-Rh/SWCNH (784.0 mA·mg^{-1}) > 30%-Rh/SWCNH (523.7 mA·mg^{-1}) > 40%-Rh/SWCNH (450.5 mA·mg^{-1}) > 10%-Rh/SWCNH (408.0 mA·mg^{-1}), similar to the ECSA trend. Meanwhile, the ECSA-normalized specific activity of 20%-Rh/SWCNH electrode is determined to be 0.76 mA·cm^{-2}, much higher than those of other reference electrodes (Fig. S6). In addition, the mass activity of the optimized 20%-Rh/SWCNH catalyst is also more competitive than that of 20%-Rh/RGO (290.9 mA·mg^{-1}), 20%-Rh/CNT (216.5 mA·mg^{-1}), 20%-Rh/C (161.2 mA·mg^{-1}), as well as the recent state-of-the-art Rh-based catalysts, such as

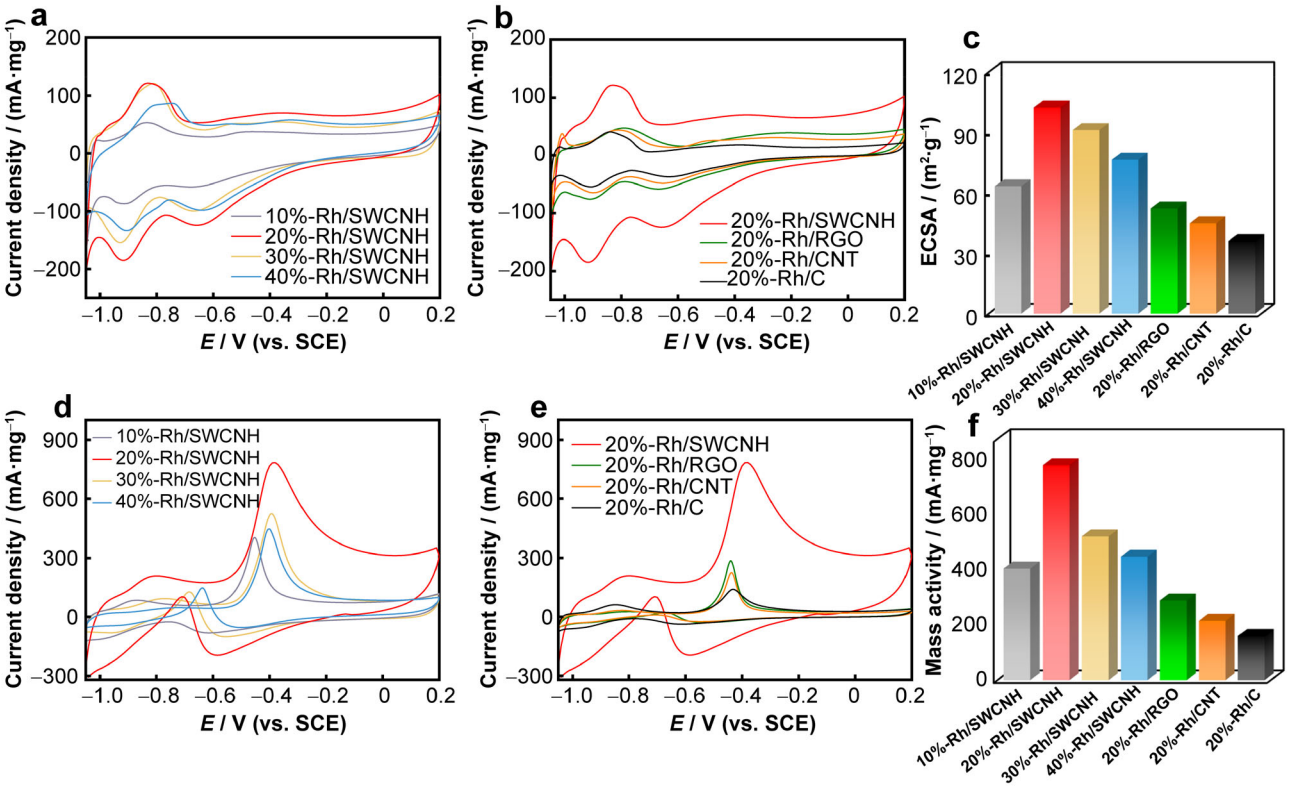

Fig. 4 CVs of **a** Rh/SWCNH catalysts with different Rh dosages and **b** 20%-Rh/RGO, 20%-Rh/CNT, and 20%-Rh/C in 1 mol·L^{-1} KOH solution at 50 mV·s^{-1}; **c** ECSA values of various catalysts; CVs of **d** Rh/SWCNH catalysts with different Pd dosages and **e** 20%-Rh/RGO, 20%-Rh/CNT, and 20%-Rh/C in 1 mol·L^{-1} KOH with 1 mol·L^{-1} CH_3OH solution at 50 mV·s^{-1}; **f** mass activities of various catalysts

graphene-supported Rh [24, 44], porous Rh nanosheets [45], Rh-based dendrites [46] and bimetallic Rh-based alloy [47] (Fig. 4e, f and Table S2). The superior methanol oxidation performance of the Rh/SWCNH catalysts should be attributed not only to the homogeneous dispersion of small-sized Rh nanoparticles, but also to the high chemical activity of SWCNHs with interconnected porous features.

In order to gain more insights into the practicability of the Rh/SWCNH catalyst, chronoamperometric technique was employed to examine its long-term electrocatalytic stability for 3000 s. As displayed in Fig. 5a, b, with a constant electrode potential, the methanol oxidation currents on all electrodes are obviously attenuated over the time due to the adsorption of CO poisoning species on the active Rh sites. Impressively, among these investigated electrodes, the 20%-Rh/SWCNH electrode maintains the highest oxidation current as well as the lowest decay rate (∼ 25% loss) during the whole test process, giving the most outstanding durability for methanol electrooxidation, which is probably linked to the strong Rh-SWCNH electronic interaction that can keep the Rh nanoparticles clean and at the same time prevent them from agglomeration, dissolution as well as Ostwald ripening. Figure S7 depicts TEM images of the 20%-Rh/SWCNH catalyst subjected to the chronoamperometric test, where the dispersion and average size of the SWCNH-supported Rh nanoparticles remain unchanged after long-term reaction, testifying its good structural stability.

The improved anti-poisoning ability of the Rh/SWCNH catalyst was further validated by the CO-stripping tests. As clearly seen from Fig. S8, the 20%-Rh/SWCNH electrode shows relatively low onset and peak potentials of CO oxidation when compared with the 20%-Rh/RGO, 20%-Rh/CNT, and 20%-Rh/C electrodes, unraveling that the utilization of SWCNHs as supports is favorable for eliminating the byproducts on the Rh sites. Additionally, the difference in the electrical conductivity between Rh/SWCNH and conventional Rh/C catalysts was investigated by the AC impedance measurements. As can be seen from Fig. 5c, d, based on the semicircle diameters, the charge-transfer resistance of 20%-Rh/SWCNH (15.8 Ω) is found to

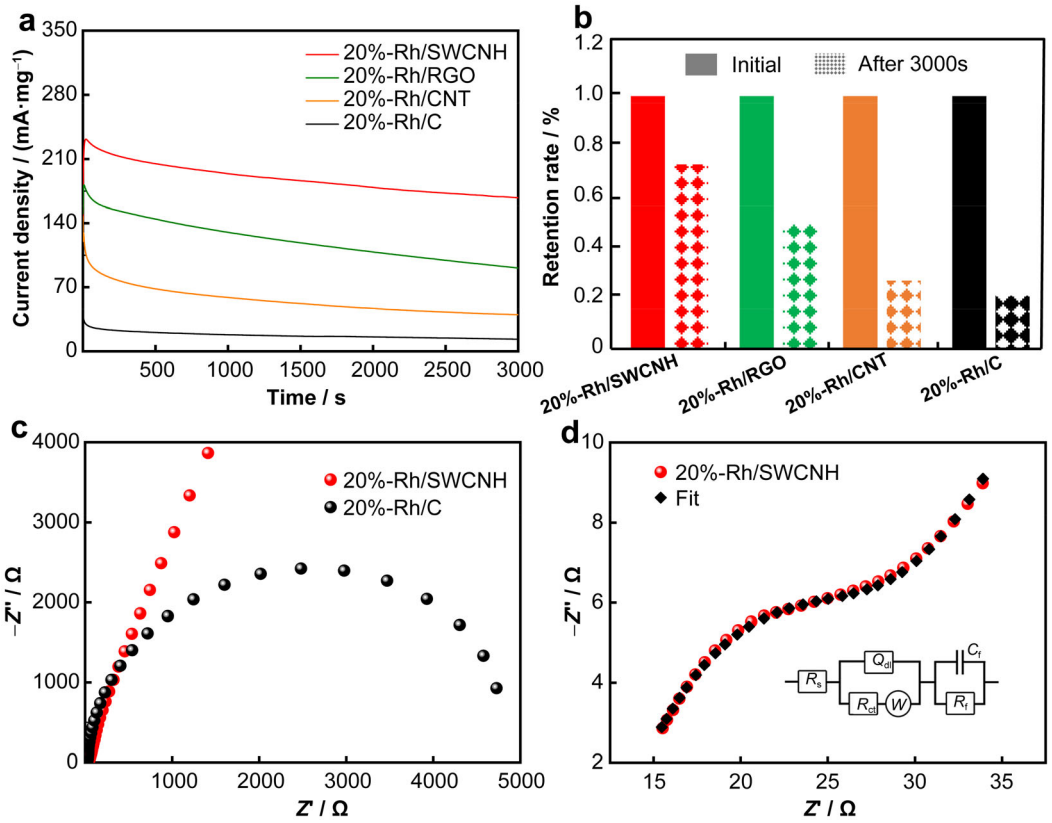

Fig. 5 **a** Chronoamperometric curves of different catalysts recorded in 1 mol·L^{-1} KOH with 1 mol·L^{-1} CH_3OH solution at − 0.5 V (vs. SCE); **b** methanol oxidation mass activities of various electrodes before and after chronoamperometry tests; **c**, **d** AC impedance spectra of 20%-Rh/SWCNH, and 20%-Rh/C catalysts collected in 1 mol·L^{-1} KOH with 1 mol·L^{-1} CH_3OH solution (inset of **d** being corresponding equivalent circuit)

be much smaller than that of 20%-Rh/C (4813.0 Ω), which can endow the catalytic system with a large population of the triple-phase boundaries for the rapid methanol oxidation kinetics.

Besides, the electrocatalytic properties of the Rh/SWCNH catalyst were further compared with those of more widely used 20%-Pt/C and 20%-Pd/C catalysts to assess its commercial prospect. Under the same test conditions, the ECSA values of the 20%-Pt/C and 20%-Pd/C catalysts are calculated to be 71.4 and 58.8 $m^2 \cdot g^{-1}$, respectively, which are less competitive than that of the 20%-Rh/SWCNH catalyst (Fig. 6a). Moreover, the methanol oxidation tests further revealed that the mass and specific activities of the 20%-Rh/SWCNH catalyst are obviously higher than those of 20%-Pt/C and 20%-Pd/C (Fig. 6b, c and Fig. S9), attesting a better catalytic efficiency for 20%-Rh/SWCNH. In addition, both chronoamperometric and continuous CV tests demonstrated that 20%-Rh/SWCNH could provide more sustainable electrocatalytic performance than 20%-Pt/C and 20%-Pd/C (Fig. 6d and Fig. S10), which is very conducive to prolonging the service life of the fuel cell devices.

4 Conclusion

In summary, the controllable synthesis of nanosized Rh grown on SWCNH matrix has been achieved through a facile and cost-effective approach. Due to their distinctive textural features including large specific surface areas, interconnected open-pore nature, optimized electronic structures, homogeneous Rh dispersion, and high electrical conductivity, the as-derived Rh/SWCNH hybrids possess large ECSA values, high mass activity, and good long-term stability toward alkaline methanol oxidation reaction, significantly superior to those of conventional Rh/C, Rh/CNT, Rh/RGO as well as commercial Pt/C and Pd/C catalysts. Such kinds of transition metal-decorated SWCNH catalysts are also expected to hold great potential for other energy- and environment-related applications beyond fuel cells, such as metal-air batteries, sensors, and photocatalysis.

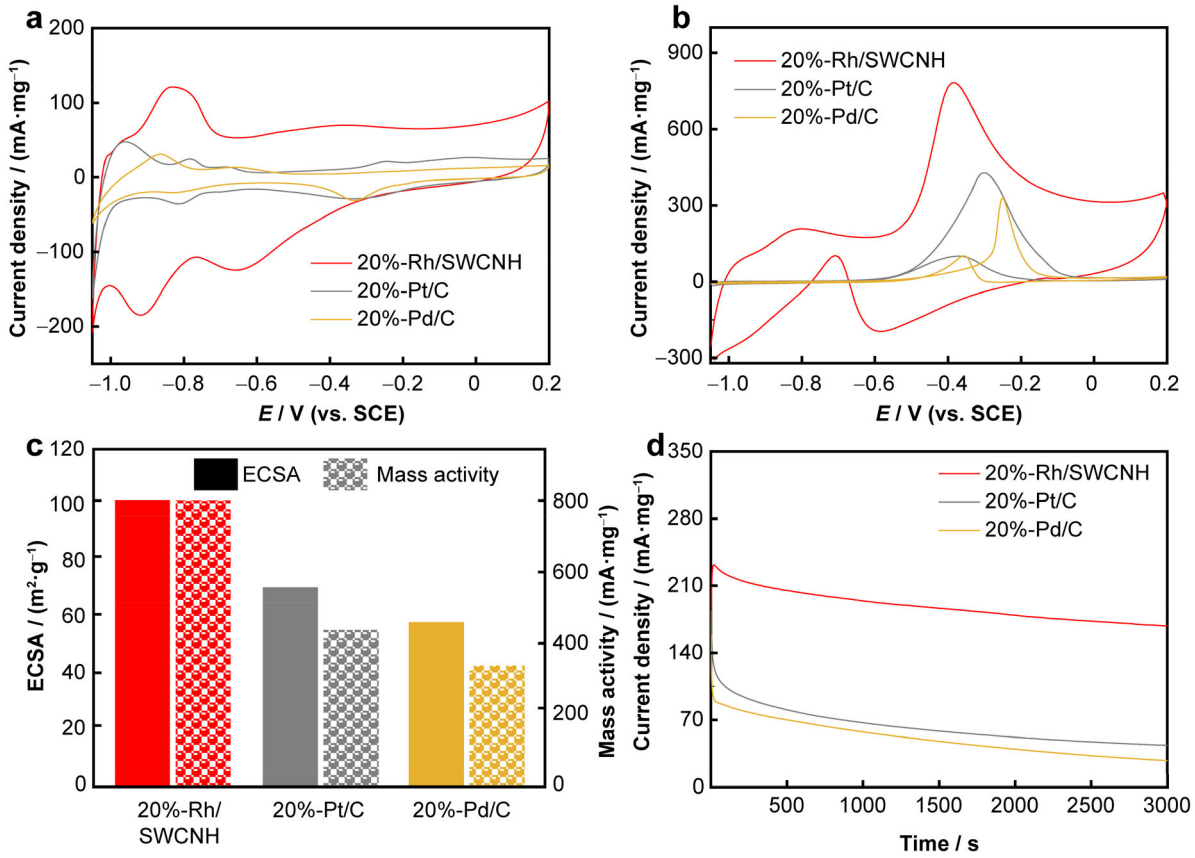

Fig. 6 CV curves of 20%-Rh/SWCNH, 20%-Pt/C, and 20%-Pd/C in **a** 1 mol·L^{-1} KOH solution and **b** 1 mol·L^{-1} KOH with 1 mol·L^{-1} CH_3OH solution at 50 mV·s^{-1}; **c** ECSA and mass activities of these three catalysts; **d** chronoamperometric curves of different catalysts recorded in 1 mol·L^{-1} KOH with 1 mol·L^{-1} CH_3OH solution

Acknowledgments This study was financially supported by the National Natural Science Foundation of China (No. 51802077) and the Fundamental Research Funds for the Central Universities (No. B210202093).

Declarations

Conflict of interests The authors declare that they have no conflict of interest.

References

[1] Chu S, Majumdar A. Opportunities and challenges for a sustainable energy future. Nature. 2012;488(7411):294.

[2] Huang HJ, Yan MM, Yang CZ, He HY, Jiang QG, Yang L, Lu ZY, Sun ZQ, Xu XT, Bando Y, Yamauchi Y. Graphene nanoarchitectonics: recent advances in graphene-based electrocatalysts for hydrogen evolution reaction. Adv Mater. 2019;31(48):1903415.

[3] Xiao WP, Bukhvalov D, Zou ZY, Zhang L, Lin ZX, Yang XF. Unveiling the origin of the high catalytic activity of ultrathin 1T/2H $MoSe_2$ nanosheets for the hydrogen evolution reaction: a combined experimental and theoretical study. Chemsuschem. 2019;12(22):5015.

[4] Xiao WP, Zhang L, Bukhvalov D, Chen ZP, Zou ZY, Shang L, Yang XF, Yan DQ, Han FY, Zhang TR. Hierarchical ultrathin carbon encapsulating transition metal doped MoP electrocatalysts for efficient and pH-universal hydrogen evolution reaction. Nano Energy. 2020;70:104445.

[5] Huang HJ, Wei YJ, Yang Y, Yan MM, He HY, Jiang QG, Yang XF, Zhu JX. Controllable synthesis of grain boundary-enriched Pt nanoworms decorated on graphitic carbon nanosheets for ultrahigh methanol oxidation catalytic activity. J Energy Chem. 2021;57:601.

[6] Yang CZ, Huang HJ, He HY, Yang L, Jiang QG, Li WH. Recent advances in MXene-based nanoarchitectures as electrode materials for future energy generation and conversion applications. Coordin Chem Rev. 2021;435:213806.

[7] Yang Y, Huang HJ, Shen BF, Jin L, Jiang QG, Yang L, He HY. Anchoring nanosized Pd on three-dimensional boron- and nitrogen-codoped graphene aerogels as a highly active multifunctional electrocatalyst for formic acid and methanol oxidation reactions. Inorg Chem Front. 2020;7(3):700.

[8] Gao ZQ, Li MM, Wang JY, Zhu JX, Zhao XM, Huang HJ, Zhang JF, Wu YP, Fu YS, Wang X. Pt nanocrystals grown on three-dimensional architectures made from graphene and MoS_2 nanosheets: highly efficient multifunctional electrocatalysts toward hydrogen evolution and methanol oxidation reactions. Carbon. 2018;139:369.

[9] Li SW, Ma SZ, Zhang YX, Zhao LM, Yang HL, Jin RF. Metal-organic interface engineering for coupling palladium nanocrystals over functionalized graphene as an advanced electrocatalyst of methanol and ethanol oxidation. J Colloid Interface Sci. 2021;588:384.

[10] Huang HJ, Guo XJ, Yan MM, Meng W, Xue Y, Xiao D, Jiang QG, Yang L, He HY. Well-dispersive Pt nanoparticles grown on 3D nitrogen- and sulfur-codoped graphene nanoribbon architectures: highly active electrocatalysts for methanol oxidation. Mater Today Energy. 2021;21:100814.
[11] Xu ML. Electrocatalytic performance of Pd–Ni nanowire arrays electrode for methanol electrooxidation in alkaline media. Rare Met. 2014;33(1):65.
[12] Li SW, Shu JH, Ma SZ, Yang HL, Jin J, Zhang XH, Jin RF. Engineering three-dimensional nitrogen-doped carbon black embedding nitrogen-doped graphene anchoring ultrafine surface-clean Pd nanoparticles as efficient ethanol oxidation electrocatalyst. Appl Catal B. 2021;280:119464.
[13] Li YR, Li MX, Li SN, Liu YJ, Chen J, Wang Y. A review of energy and environment electrocatalysis based on high-index faceted nanocrystals. Rare Met. 2021;40(12):3406.
[14] Yang CZ, He HY, Jiang QG, Liu XY, Shah SP, Huang HJ, Li WH. Pd nanocrystals grown on MXene and reduced graphene oxide co-constructed three-dimensional nanoarchitectures for efficient formic acid oxidation reaction. Int J Hydrogen Energy. 2021;46(1):589.
[15] Wu YN, Liao SJ, Guo HF, Hao XY, Liang ZX. Ultralow platinum-loading PtPdRu@PtRuIr/C catalyst with excellent CO tolerance and high performance for the methanol oxidation reaction. Rare Met. 2013;33(3):337.
[16] Liu DB, Li XY, Chen SM, Yan H, Wang CD, Wu CQ, Haleem YA, Duan S, Lu JL, Ge BH, Ajayan PM, Luo Y, Jiang J, Song L. Atomically dispersed platinum supported on curved carbon supports for efficient electrocatalytic hydrogen evolution. Nat Energy. 2019;4(6):512.
[17] Yan MM, Jiang QG, Zhang T, Wang JY, Yang L, Lu ZY, He HY, Fu YS, Wang X, Huang HJ. Three-dimensional low-defect carbon nanotube/nitrogen-doped graphene hybrid aerogel-supported Pt nanoparticles as efficient electrocatalysts toward the methanol oxidation reaction. J Mater Chem A. 2018;6(37):18165.
[18] Yang CZ, Jiang QG, Liu H, Yang L, He HY, Huang HJ, Li WH. Pt-on-Pd bimetallic nanodendrites stereoassembled on MXene nanosheets for use as high-efficiency electrocatalysts toward the methanol oxidation reaction. J Mater Chem A. 2021;9(27):15432.
[19] Yang CZ, Jiang QG, Huang HJ, He HY, Yang L, Li WH. Polyelectrolyte-induced stereoassembly of grain boundary-enriched platinum nanoworms on $Ti_3C_2T_X$ MXene nanosheets for efficient methanol oxidation. ACS Appl Mater Interfaces. 2020;12(21):23822.
[20] Shu JH, Li RX, Lian ZM, Zhang W, Jin RF, Yang HL, Li SW. In-situ oxidation of palladium–iridium nanoalloy anchored on nitrogen-doped graphene as an efficient catalyst for methanol electrooxidation. J Colloid Interface Sci. 2022;605:44.
[21] Xu ML, Yang XK, Zhang YJ, Xia SB, Dong P, Yang GT. Enhanced methanol oxidation activity of Au@Pd nanoparticles supported on MWCNTs functionalized by MB under ultraviolet irradiation. Rare Met. 2014;34(1):12.
[22] He Q, Tian D, Jiang HL, Cao DF, Wei SQ, Liu DB, Song P, Lin Y, Song L. Achieving efficient alkaline hydrogen evolution reaction over a Ni_5P_4 catalyst incorporating single-atomic Ru sites. Adv Mater. 2020;32(11):1906972.
[23] Lu Y, Fan DQ, Chen ZP, Xiao WP, Cao CC, Yang XF. Anchoring Co_3O_4 nanoparticles on MXene for efficient electrocatalytic oxygen evolution. Sci Bull. 2020;65(6):460.
[24] Yang Y, Song YX, Sun H, Xiang DY, Jiang QG, Lu ZY, He HY, Huang HJ. Rh-decorated three-dimensional graphene aerogel networks as highly-efficient electrocatalysts for direct methanol fuel cells. Front Energy Res. 2020;8:60.
[25] Xiong Y, Dong JC, Huang ZQ, Xin PY, Chen WX, Wang Y, Li Z, Jin Z, Xing W, Zhuang ZB, Ye JY, Wei X, Cao R, Gu L, Sun SG, Zhuang L, Chen XQ, Yang H, Chen C, Peng Q, Chang CR, Wang DS, Li YD. Single-atom Rh/N-doped carbon electrocatalyst for formic acid oxidation. Nat Nanotechnol. 2020;15(5):390.
[26] Ge JJ, Yin PQ, Chen Y, Cheng HF, Liu JW, Chen B, Tan CL, Yin PF, Zheng HX, Li QQ, Chen SM, Xu WJ, Wang XQ, Wu G, Sun RB, Shan XH, Hong X, Zhang H. Ultrathin amorphous/crystalline heterophase Rh and Rh alloy nanosheets as tandem catalysts for direct indole synthesis. Adv Mater. 2021;33(9):2006711.
[27] Yang CZ, Jiang QG, Li WH, He HY, Yang L, Lu ZY, Huang HJ. Ultrafine Pt nanoparticle-decorated 3D hybrid architectures built from reduced graphene oxide and MXene nanosheets for methanol oxidation. Chem Mater. 2019;31(22):9277.
[28] Zhou YZ, Tao XF, Chen GB, Lu RH, Wang D, Chen MX, Jin EQ, Yang J, Liang HW, Zhao Y, Feng XL, Narita A, Müllen K. Multilayer stabilization for fabricating high-loading single-atom catalysts. Nat Commun. 2020;11(1):5892.
[29] Li Y, Li X, Pillai HS, Lattimer J, Mohd AN, Karakalos S, Chen MJ, Guo L, Xu H, Yang J, Su D, Xin HL, Wu G. Ternary PtIrNi catalysts for efficient electrochemical ammonia oxidation. ACS Catal. 2020;10(7):3945.
[30] Yang Y, Huang HJ, Yang CZ, He HY. Ultrafine Rh-decorated 3D porous boron and nitrogen dual-doped graphene architecture as an efficient electrocatalyst for methanol oxidation reaction. ACS Appl Energy Mater. 2021;4(1):376.
[31] Liu S, Wang X, Yu HG, Wu YP, Li B, Lan YQ, Wu T, Zhang J, Li DS. Two new pseudo-isomeric nickel (II) metal–organic frameworks with efficient electrocatalytic activity toward methanol oxidation. Rare Met. 2021;40(2):489.
[32] Huang HJ, Wang X. Recent progress on carbon-based support materials for electrocatalysts of direct methanol fuel cells. J Mater Chem A. 2014;2(18):6266.
[33] Liu MM, Zhang RZ, Chen W. Graphene-supported nanoelectrocatalysts for fuel cells: synthesis, properties, and applications. Chem Rev. 2014;114(10):5117.
[34] Huang HJ, Zhu JX, Zhang WY, Tiwary CS, Zhang JF, Zhang X, Jiang QG, He HY, Wu YP, Huang W, Ajayan PM, Yan QY. Controllable codoping of nitrogen and sulfur in graphene for highly efficient Li-oxygen batteries and direct methanol fuel cells. Chem Mater. 2016;28(6):1737.
[35] Ren JX, Zhang J, Yang CZ, Yang Y, Zhang YF, Yang FX, Ma RQ, Yang L, He HY, Huang HJ. Pd nanocrystals anchored on 3D hybrid architectures constructed from nitrogen-doped graphene and low-defect carbon nanotube as high-performance multifunctional electrocatalysts for formic acid and methanol oxidation. Mater Today Energy. 2020;16:100409.
[36] Li Y, Wen HJ, Yang J, Zhou YZ, Cheng X. Boosting oxygen reduction catalysis with N, F, and S tri-doped porous graphene: tertiary N-precursors regulates the constitution of catalytic active sites. Carbon. 2019;142:1.
[37] Karousis N, Suarez-Martinez I, Ewels CP, Tagmatarchis N. Structure, properties, functionalization, and applications of carbon nanohorns. Chem Rev. 2016;116(8):4850.
[38] Zhu CX, Liu D, Chen Z, Li LB, You TY. Superior catalytic activity of Pt/carbon nanohorns nanocomposites toward methanol and formic acid oxidation reactions. J Colloid Interface Sci. 2018;511:77.
[39] Guo XJ, Yang L, Shen BF, Wei YJ, Yang Y, Yang CZ, Jiang QG, He HY, Huang HJ. Ultrafine Pd nanocrystals anchored onto single-walled carbon nanohorns: a highly-efficient multifunctional electrocatalyst with ultra-low Pd loading for formic acid and methanol oxidation. Mater Chem Phys. 2020;250:123167.

[40] Niu B, Xu W, Guo ZD, Zhou NZ, Liu Y, Shi ZJ, Lian YF. Controllable deposition of platinum nanoparticles on single-wall carbon nanohorns as catalyst for direct methanol fuel cells. J Nanosci Nanotechnol. 2012;12(9):7376.
[41] Zhu SY, Xu GB. Single-walled carbon nanohorns and their applications. Nanoscale. 2010;2(12):2538.
[42] Berber S, Kwon YK, Tomanek D. Electronic and structural properties of carbon nanohorns. Phys Rev B. 2000;62(4):2291.
[43] Halder A, Sharma S, Hegde MS, Ravishankar N. Controlled attachment of ultrafine platinum nanoparticles on functionalized carbon nanotubes with high electrocatalytic activity for methanol oxidation. J Phys Chem C. 2009;113(4):1466.
[44] Kang YQ, Xue Q, Jin PJ, Jiang JX, Zeng JH, Chen Y. Rhodium nanosheets–reduced graphene oxide hybrids: a highly active platinum-alternative electrocatalyst for the methanol oxidation reaction in alkaline media. ACS Sustain Chem Eng. 2017;5(11):10156.
[45] Zhu JY, Chen SQ, Xue Q, Li FM, Yao HC, Xu L, Chen Y. Hierarchical porous Rh nanosheets for methanol oxidation reaction. Appl Catal B. 2020;264:118520.
[46] Kang YQ, Li FM, Li SN, Ji PJ, Zeng JH, Jiang JX, Chen Y. Unexpected catalytic activity of rhodium nanodendrites with nanosheet subunits for methanol electrooxidation in an alkaline medium. Nano Res. 2016;9(12):3893.
[47] Wang ZQ, Zhang HG, Liu SL, Dai ZC, Wang P, Xu Y, Li XN, Wang L, Wang HJ. Engineering bunched RhTe nanochains for efficient methanol oxidation electrocatalysis. Chem Commun. 2020;56(88):13595.